

SANDIA REPORT

SAND 2007-5361

Unlimited Release

Printed October 2007

Non Destructive Testing of Test Objects

Bernice E. Mills

Prepared by
Sandia National Laboratories
Albuquerque, New Mexico 87185 and Livermore, California 94550

Sandia is a multiprogram laboratory operated by Sandia Corporation,
a Lockheed Martin Company, for the United States Department of Energy's
National Nuclear Security Administration under Contract DE-AC04-94-AL85000.

Approved for public release; further dissemination unlimited.



Sandia National Laboratories

Issued by Sandia National Laboratories, operated for the United States Department of Energy by Sandia Corporation.

NOTICE: This report was prepared as an account of work sponsored by an agency of the United States Government. Neither the United States Government, nor any agency thereof, nor any of their employees, nor any of their contractors, subcontractors, or their employees, make any warranty, express or implied, or assume any legal liability or responsibility for the accuracy, completeness, or usefulness of any information, apparatus, product, or process disclosed, or represent that its use would not infringe privately owned rights. Reference herein to any specific commercial product, process, or service by trade name, trademark, manufacturer, or otherwise, does not necessarily constitute or imply its endorsement, recommendation, or favoring by the United States Government, any agency thereof, or any of their contractors or subcontractors. The views and opinions expressed herein do not necessarily state or reflect those of the United States Government, any agency thereof, or any of their contractors.

Printed in the United States of America. This report has been reproduced directly from the best available copy.

Available to DOE and DOE contractors from
U.S. Department of Energy
Office of Scientific and Technical Information
P.O. Box 62
Oak Ridge, TN 37831

Telephone: (865) 576-8401
Facsimile: (865) 576-5728
E-Mail: reports@adonis.osti.gov
Online ordering: <http://www.doe.gov/bridge>

Available to the public from
U.S. Department of Commerce
National Technical Information Service
5285 Port Royal Rd
Springfield, VA 22161

Telephone: (800) 553-6847
Facsimile: (703) 605-6900
E-Mail: orders@ntis.fedworld.gov
Online order: <http://www.ntis.gov/help/ordermethods.asp?loc=7-4-0#online>



SAND 2007-5361
Unlimited Release
Printed October 2007

Non Destructive Testing of Test Objects

Bernice E. Mills
Materials Chemistry Department
Sandia National Laboratories
P.O. Box 969
Livermore, California-9403

Abstract

In order to determine the visibility of various features by different techniques and in different settings, several test objects containing wires have been used as standards. Examples are shown of the use of x-ray and active thermal imaging for the detection of inclusions. The effect of x-ray accelerating voltage and confounding materials on the x-ray images is shown. Calculated transmission functions for selected materials at a range of voltages are given. The effect of confounding materials, finishes, and textures on thermography is shown and on x-radiography is discussed.

This page intentionally left blank.

Contents

| | |
|--|----|
| Abstract | 3 |
| Introduction | 9 |
| X-ray results and discussion | 9 |
| Thermography results and discussion..... | 17 |
| Conclusion | 19 |
| Distribution | 21 |

This page intentionally left blank.

List of Figures

| | | |
|------------|--|----|
| Figure 1. | X-ray images of 0.02 cm Al 2024-O wire immobilized in fiberglass. | 10 |
| Figure 2. | Calculated transmission function of a narrow beam of x-rays through 0.02 cm of Al 2024-O as a function of x-ray energy up to 130 keV..... | 10 |
| Figure 3. | Left: 130 keV, 40sec x-ray image from Figure 1 compared with Right: x-ray image at 320 keV, 10 sec. | 11 |
| Figure 4. | Comparison of the transmission function for 0.02 cm Al 2024-O (solid red) with that for 2 cm of the same alloy (blue dashed).. | 12 |
| Figure 5. | Measured film density at two accelerating voltages for aluminum. Optimum film density is in the range of 2 to 2.5..... | 13 |
| Figure 6. | Calculated transmission function for (from left to right at $I/I_0 = 0.5$) 0.02 cm Al 2024-O (red), 0.015 cm Cu (blue), 0.148 cm Al (black), and 0.148 cm Beralcast 363-based alloy modified to contain 10 wt.% Be (green)..... | 14 |
| Figure 7. | X-ray images of (from left to right) 0.148 cm Al, 0.148 cm Beralcast 363-based alloy modified to contain 10 wt.% Be, 0.015 cm Cu, and (visible in the right-hand image only) 0.02 cm Al 2024-O.. | 15 |
| Figure 8. | X-ray images taken at 30 kV. Left is contact print; right, taken with an object-to-film distance of 1.1". | 16 |
| Figure 9. | Transmission function for (from let to right) S2 glass (blue), E glass (red), and 50% lead glass (black)..... | 17 |
| Figure 10. | Optical image and active thermographs of Al 2024-O wires embedded in fiberglass. A: optical image of "front" side..... | 18 |
| Figure 11. | Higher magnification image of object from Figure 8 showing the numerous bubbles embedded in the fiberglass that are not visible in the thermographs. | 19 |

This page intentionally left blank.

Non Destructive Testing of Test Objects

Introduction

Several test objects were made to evaluate the effectiveness of non-destructive evaluation techniques in visualizing contaminants and inclusions. The principle technique evaluated was x-radiography. Active thermography was also used in some cases. Ultrasonics was considered and rejected as unwieldy as well as being poorly suited to visualize small features. The objects all contained or simulated metallic inclusions, so x-ray was considered appropriate for this application.

The ability to distinguish one material on another material is a function of their composition and thickness as well as the energy of the x-ray. Transmission function calculations can help to illustrate the effect of specimen thickness and x-ray accelerating voltage on the number of photons that penetrate a given material. These calculations were done using PhotoKoef, a nuclear physics utilities program from AIC Software, Inc. of Grafton, MA. In practical terms we must also consider the time necessary to acquire an image and the access to the material or surface of interest.

Thermography has other considerations. It is not sensitive to material atomic number, but rather its properties of absorption, reflection, transmission, and conduction. As such it represents an independent method of inspecting materials, with its own possible difficulties.

X-ray results and discussion

The test objects simulating inclusions were all in the form of wire. The finest aerial density object used was 0.02 cm Al 2024-O wire (specified as weight percent: 90.7-94.7 Al, max 0.1 Cr, 3.8-4.9 Cu, max 0.5 Fe, 1.2-1.8 Mg, 0.3-0.9 Mn, max 0.5 Si, max 0.15 Ti, max 0.25 Zn). First the object was studied under conditions where an optimal image could be obtained. Then non-optimal conditions were used to see if it was still possible to obtain an image. An example is seen in Figure 1. The 2024-O aluminum wires were immobilized in fiberglass. The radiographs shown are contact prints that were taken with a Faxitron using a 54" source-to-film distance using bare M film. The source has a spot size of 0.5 mm and operates at 3 mA. The left image required an exposure of 15 min. at 30 keV accelerating voltage; the right, 40 sec at 130 keV. Although the excellent definition visible in the left hand image is not seen in the right image, the wires are still clearly visible. The cause of the degradation in definition is illustrated in Figure 2.

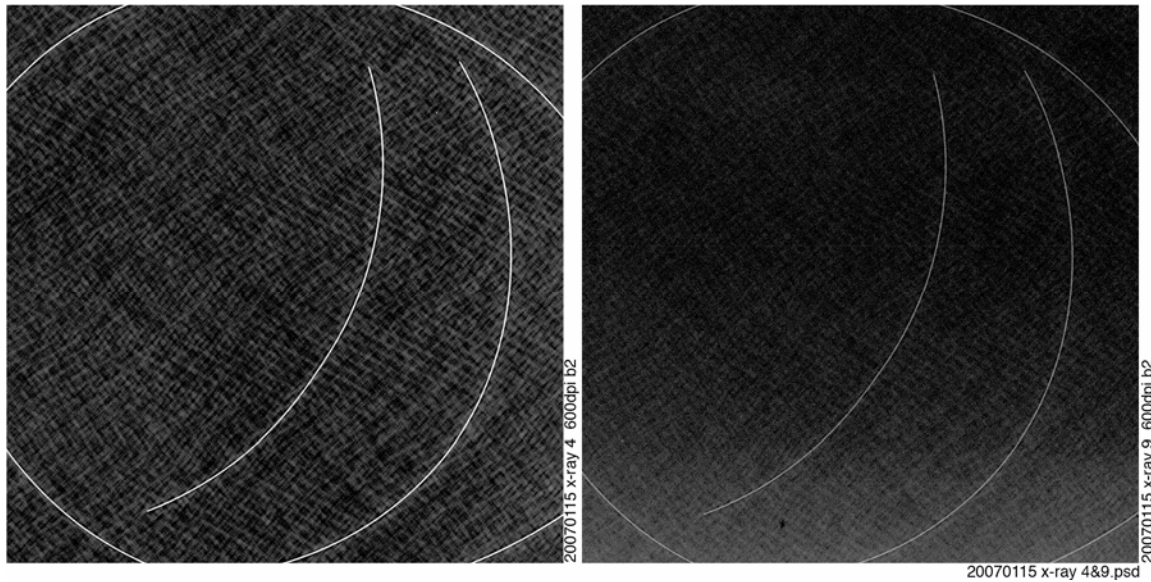


Figure 1. X-ray images of 0.02 cm Al 2024-O wire immobilized in fiberglass.
 Left: 30 keV accelerating voltage; 15 min.
 Right: 130 keV; 40 sec.

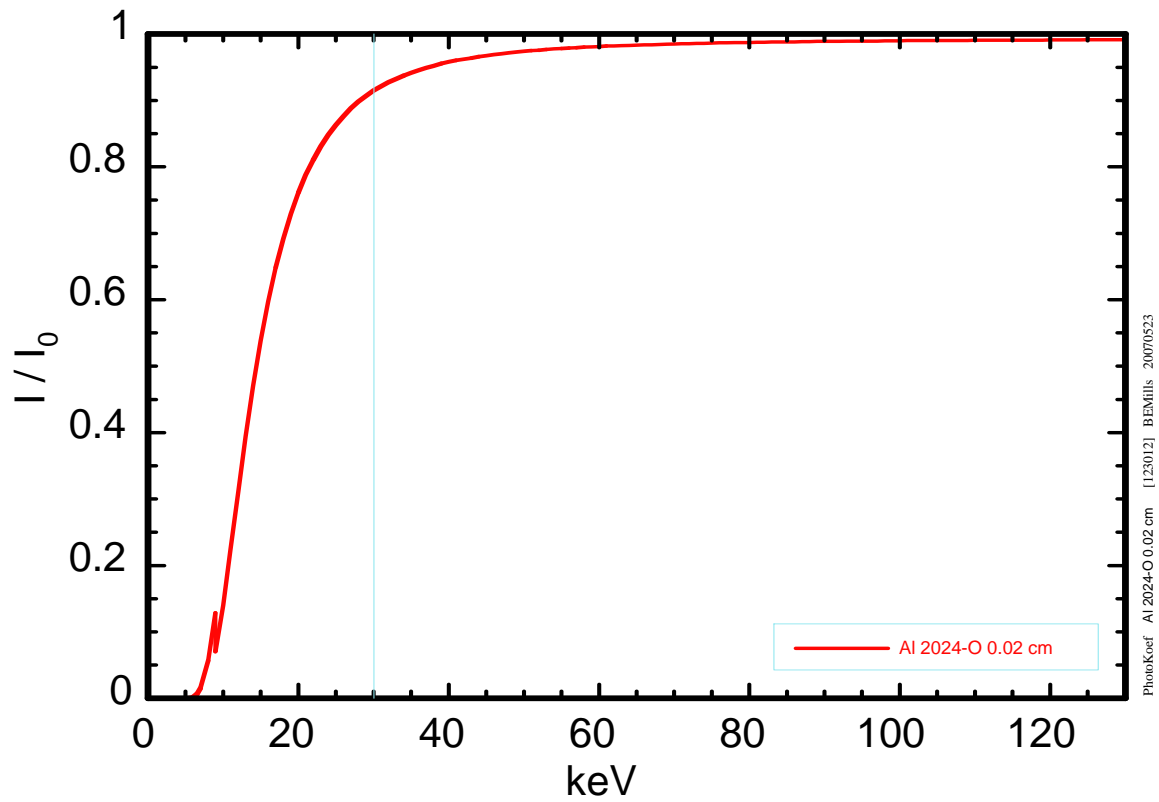


Figure 2. Calculated transmission function of a narrow beam of x-rays through 0.02 cm of Al 2024-O as a function of x-ray energy up to 130 keV.

Figure 2 shows the calculated transmission function (using PhotoKoeF) of a narrow beam of x-rays through 0.02 cm of Al 2024-O as a function of x-ray energy up to 130 keV, the accelerating voltage used for the right-hand image in Figure 1. I/I_0 is the fraction of incoming photons that penetrate through the sample. The accelerating voltage is only the highest energy x-ray in the source, so that there will be lower energy photons as well in the beam. It is clear, however, that almost all of the photons come through the sample at high energy and fewer penetrate the sample at energies below 30 keV, the accelerating voltage for the left hand image in Figure 1. This accounts for the difference in exposure time required (40 sec vs. 15 min) between the high and low energies.

Exposures taken at 320 keV yield images which are much poorer (Figure 3). These were M100 films taken in 10 sec. at 48" with a Philips 320 which had been derated to operate at 2 mA instead of 10 mA because the x-ray tube could not be cycled on and off quickly enough to give a proper exposure at the higher current. At higher energies these very small objects require smaller exposure times. In the field it is common to use radioactive sources, which are physically delivered from a storage container, or "pig", for exposure. In this case the short time for exposure is incompatible with the time needed for running the source in and out of position. Likewise, with accelerator sources which depend on a shutter to control the beam, it is difficult to cycle the shutter fast enough to obtain an image at all. For example, at the LIGA exposure station at SLAC the shutter did not cycle fast enough to get a good exposure with 0.02 cm gold using very slow x-ray film.

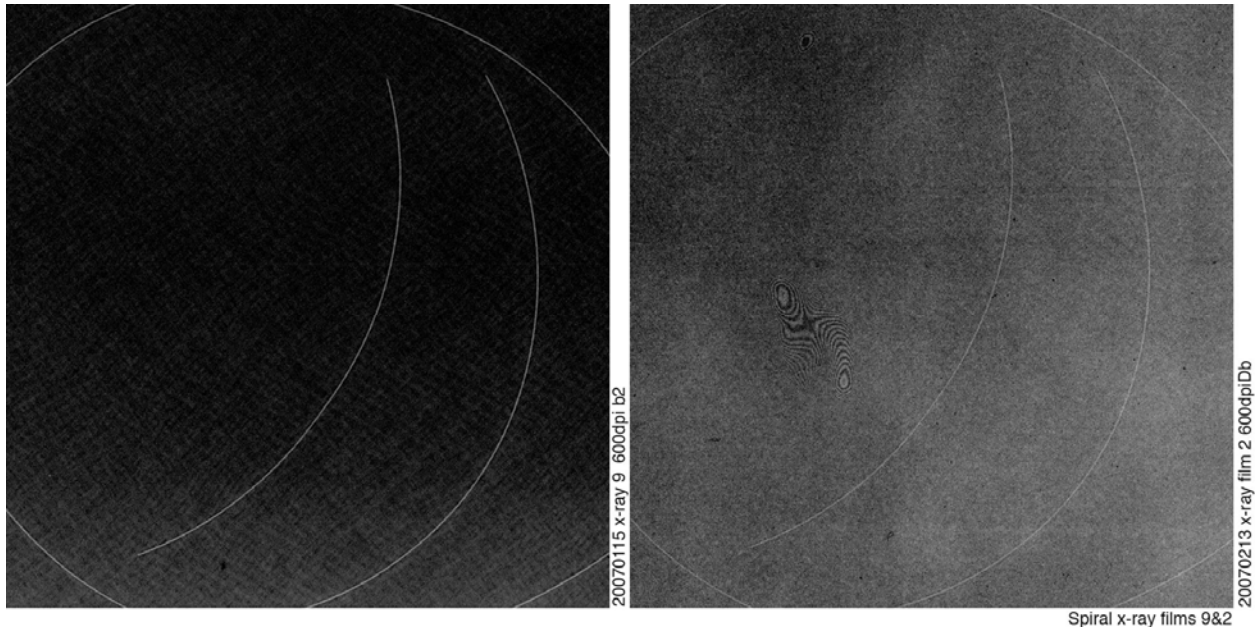


Figure 3. Left: 130 keV, 40sec x-ray image from Figure 1 compared with Right: x-ray image at 320 keV, 10 sec.

In actual conditions it is usually necessary to detect inclusions not in a stand-alone situation or immobilized in a low Z matrix, but along with more high Z material. The limit of visibility was tested in the presence of other materials. Visible only with a high intensity light is the very faint image of the 0.02 cm wire on 2 cm of aluminum. This is the limit of detection and is only possible because the wire is a recognizable object and not a point or random shaped object. The

image of the 0.02 cm wire on a 2 cm aluminum background was obtained at 130 keV at about half the source-to-film distance and with a 5 min. rather than a 40 sec. exposure as in Figure 1. Had it been at the 54" distance, it would have required about 20 min exposure. The problem of a small object or flaw on or in a thick substrate is illustrated in Figure 4. At low voltage, where we have seen we can get excellent definition, no photons get through the sample. At higher voltage there is little contrast available to image a flaw or inclusion. This contrast difference is shown in Figure 5. The optimal film density is shown with the central horizontal band. At the lower voltage, a small change in thickness results in a relatively large change in film density compared to the large thickness range that gives good density images for any given exposure at higher voltage. This makes it easier to see fine thickness changes or to visualize small inclusions at lower voltages if enough photons get through the object to create an image in a finite amount of time. The high energy in Figure 4 is that of a ^{60}Co source, an option for field use when an x-ray tube is not available. It would not be possible to image a 0.02 cm Al wire on a 2 cm Al object with a ^{60}Co source as there would not be enough contrast.

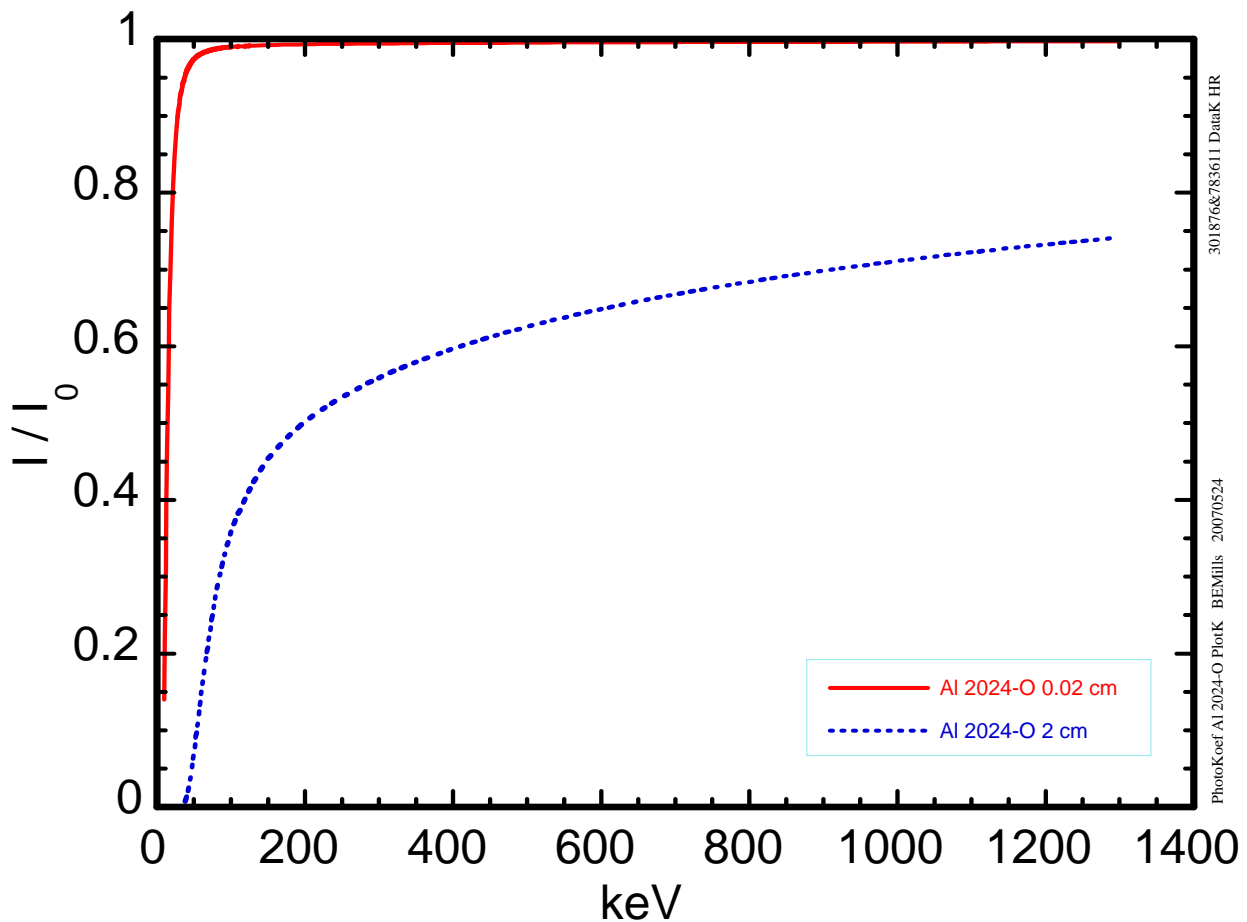


Figure 4. Comparison of the transmission function for 0.02 cm Al 2024-O (solid red) with that for 2 cm of the same alloy (blue dashed). The x-axis scale is up to the energy for ^{60}Co .

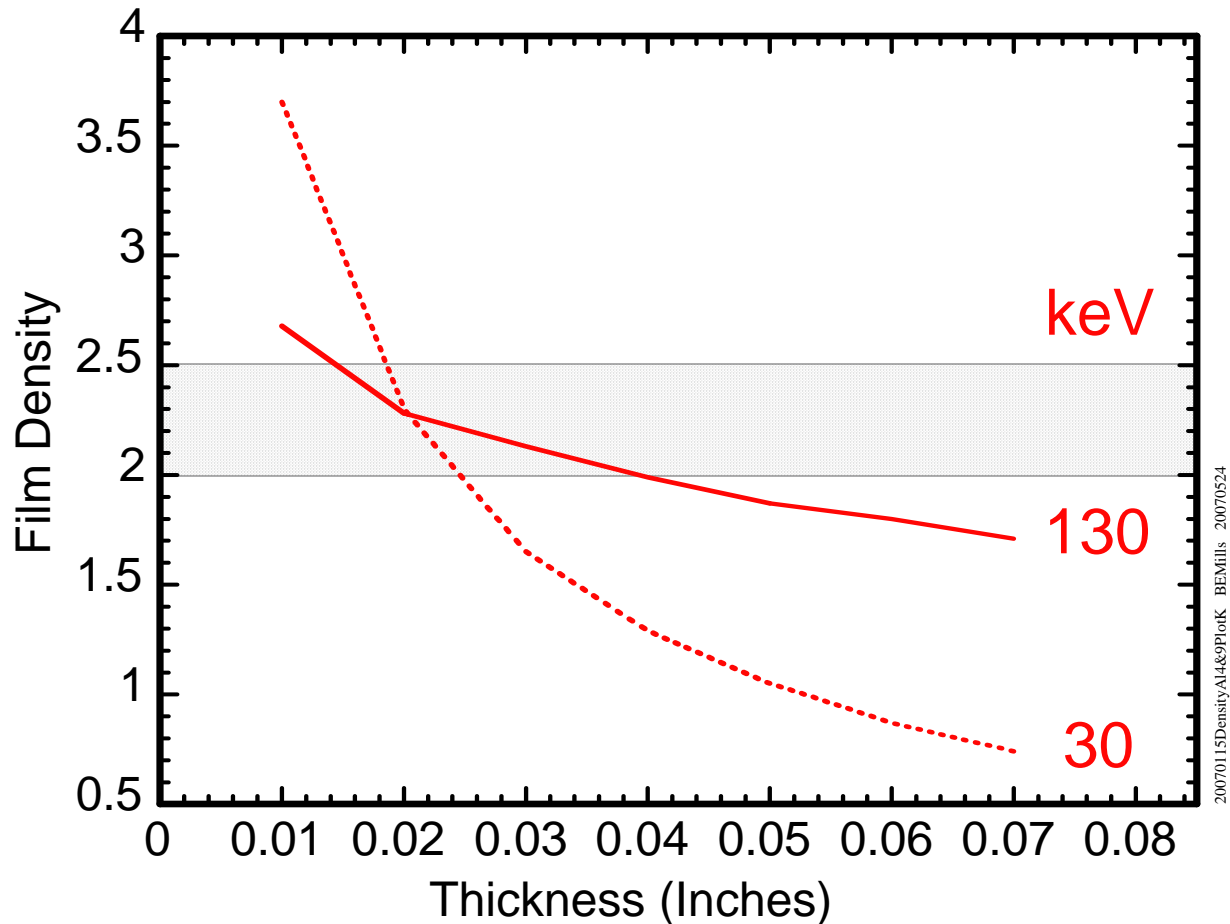


Figure 5. Measured film density at two accelerating voltages for aluminum. Optimum film density is in the range of 2 to 2.5. A small change in thickness results in a much larger change in density at 30 keV than it does at 130 keV.

When higher Z materials are introduced with the 0.02 cm Al 2024-O wire test object, it becomes more difficult to detect the object. With 0.39 cm thick stainless steel, it is not possible to detect a 0.02 cm Al wire. For higher Z materials at this or greater thickness a single test wire would also not be detected.

Other wire test objects were also used:

0.015 cm Cu

0.148 cm Al

0.148 cm a Beralcast 363-based alloy modified to contain 10 wt. % Be

[note: specifications would make the composition approximately Be 10, Al 77.8, Ag 7.68, Co 2.56, Ge 1.92 with small amounts of Si and Fe.]

The calculated transmission of these objects compared to that of the Al 2024-O wire is shown in Figure 6. All can be expected to transmit fewer x-rays at every energy than the Al alloy wire. The 10% Be Beralcast has the least transmission at every energy above the 25.5 keV K absorption edge of silver, seen in Figure 6 as a step at that energy. X-rays above this edge

have enough energy to remove a 1s electron from the silver in the Be alloy, x-rays just below this edge do not have enough energy to cause this ionization and therefore are more likely to penetrate the material. The copper K absorption is also seen just below 9 keV. In this case it is barely visible on the copper curve because there is so little transmission through the copper at that energy. The Cu K edge is more apparent on the Al 2024-O curve since Cu is a constituent of that alloy and there is still some transmission through the Al alloy at that energy. At the highest energies the copper and 10% Be Beralcast have similar transmission.

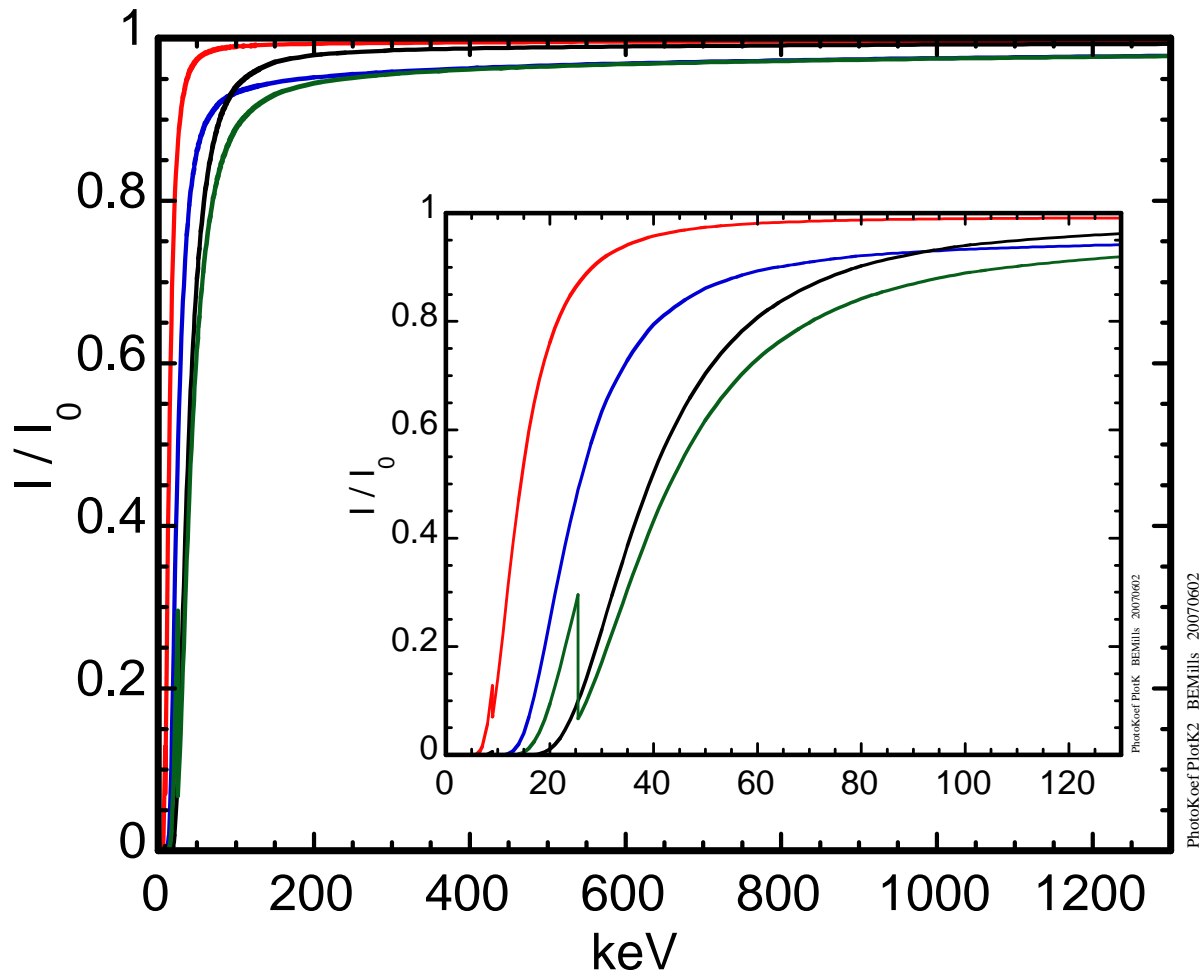


Figure 6. Calculated transmission function for (from left to right at $I/I_0 = 0.5$) 0.02 cm Al 2024-O (red), 0.015 cm Cu (blue), 0.148 cm Al (black), and 0.148 cm Beralcast 363-based alloy modified to contain 10 wt.% Be (green). Shown are two different scales: 0 to 130 keV and 0 to 1300 keV. At lower energy the two thicker Al and modified Beralcast alloy objects are expected to be more detectable, whereas at higher energy the thin Cu and the Beralcast should be more detectable.

These objects were not immobilized in fiberglass but taped to a sheet of plastic film. Figure 7 left shows an image obtained at 30 keV and 3 mA, with a 15 min. exposure at 30". At this accelerating voltage most of the x-rays must be below the 25.5 keV silver K edge because the Be alloy wire second from the left is much fainter than that of the same sized Al wire on the left. The Be alloy wire has a distinctly non-uniform appearance, indicating a high degree of

segregation of the alloying constituents into different grains. This is consistent with the material not being very ductile. The copper wire, seen to the right of the Be alloy wire, is quite prominent, but the fine Al alloy wire is not seen in this image because it is over-exposed. Although the time to expose the film is the same as that in Figure 1 left, the source to film distance is about half that. At 54" it would have taken about an hour to obtain the image in Figure 7 left. At a 130 keV accelerating voltage (Figure 7 right) behind a 0.0035" (0.0089 cm) thick steel plate, it is possible to see all of the four wires. The fine aluminum alloy wire is seen at the right of the image. Since it is difficult to see the finest Al wire on a 0.0089 cm thick steel plate, this is consistent with the inability to image this wire on a 0.39 cm thick steel substrate as noted above. Note that at this energy both the aluminum and the 10% Be Beralcast wire look very similar in contrast to their very different appearance at 30 keV.

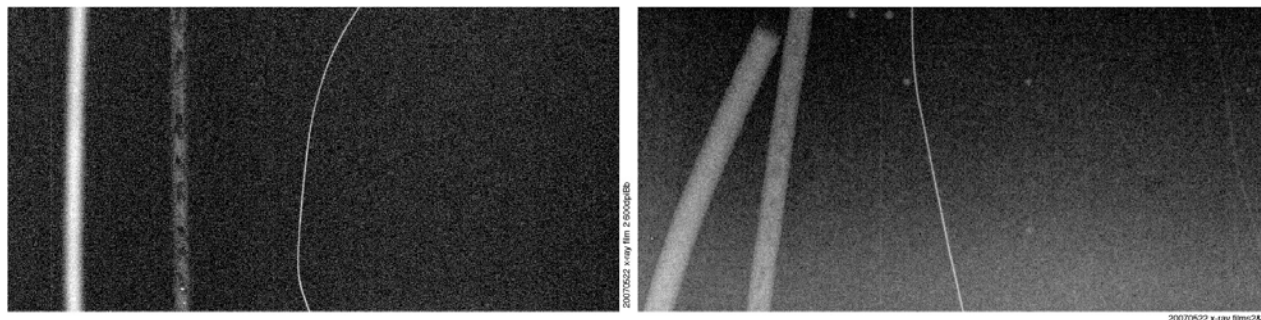


Figure 7. X-ray images of (from left to right) 0.148 cm Al, 0.148 cm Beralcast 363-based alloy modified to contain 10 wt.% Be, 0.015 cm Cu, and (visible in the right-hand image only) 0.02 cm Al 2024-O. Left taken at 30 keV; right at 130 keV and behind a 0.0089 cm thick steel plate. The fine Al wire is not visible on the left because it is overexposed, but is visible at the right of the right hand image.

Further x-ray exposures were carried out using aluminum, 304 stainless steel and tantalum sheet with 0.02 cm aluminum 2024-O and 0.022 cm copper wires. In all cases, the copper is easily visible in good images with the naked eye aided only by blocking the surrounding light on at least 1.0 inch aluminum, 0.1 inch steel, and 0.03 inch tantalum. The aluminum wire is faintly visible on 0.8 inch aluminum with the aid of blocking the surrounding light and magnification. This is consistent with the 2 cm thick aluminum substrate where the 0.02 cm wire was just barely visible as reported above. The aluminum wire was just barely detected, again with the aid of blocking the light and magnification, on a 0.09 inch steel substrate. At about 0.22 cm, this is consistent with the previous report that the 0.02 cm Al wire cannot be seen on 0.38 cm steel. There was some corrosion on the steel. The image of the corrosion is much more prominent than that of the aluminum wire. In most cases, locating the aluminum wire would be very difficult if it were not accompanied by the copper wire.

When the imaged object is not directly on the film, but at a distance from the film, the image is degraded unless the x-rays come from a point source. With a 0.5 mm source using 30 keV accelerating voltage, the image is degraded as seen in Figure 8. Left is a contact print. Right is an image taken with the object 1.1 inch from the film. Although the image of the aluminum is clear, it is also quite clearly degraded compared to the contact print. It is possible to overcome

this effect by using a microfocus x-ray source. An example of a microfocus source is the FeinFocus, which has a nominal 2 μ spot size, although it is necessary to limit the current to realize this spot size. The effect of increasing the object-to-film distance in this case is primarily to increase the magnification of the image of the object on the film.

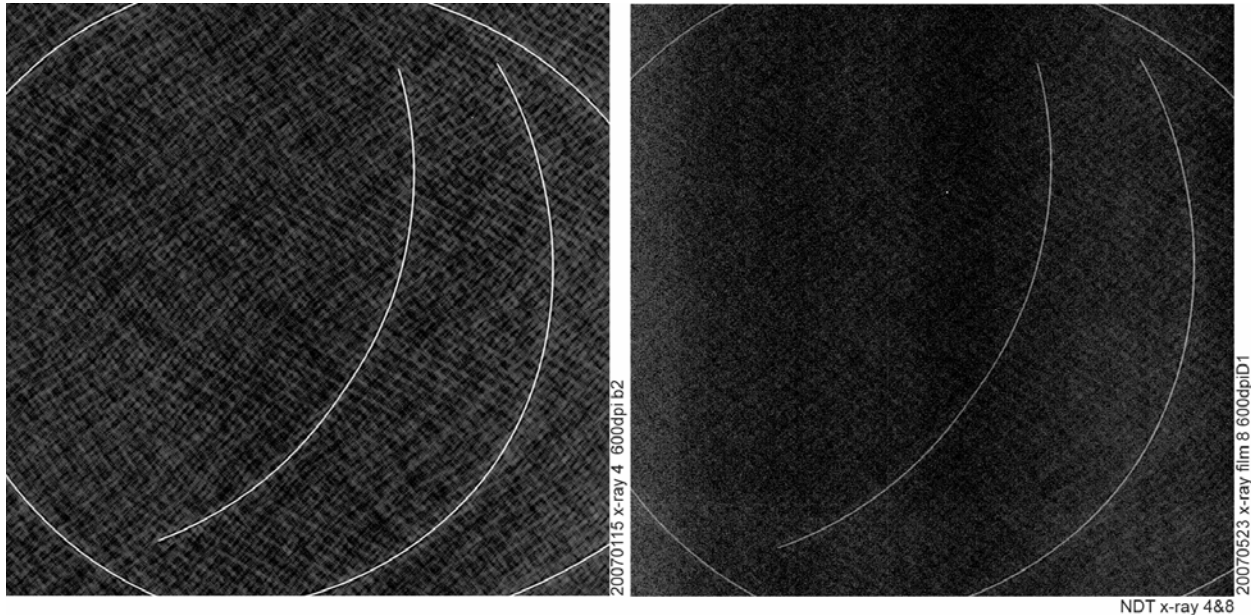


Figure 8. X-ray images taken at 30 kV. Left is contact print; right, taken with an object-to-film distance of 1.1”.

It should be noted that x-radiography is not limited to the detection of metallic inclusions. The detection limit for any particular inclusion depends on the composition and thickness of the inclusion and of the material with which it is associated. An example is seen in Figure 9. In this case we see, from left to right, the transmission curves for 3 mm of S2, E, and 50% lead glass. S2-glass is a higher strength, lower density glass. E, or electrical, glass is slightly higher density, but very similar to S2-glass. 50% lead glass is very high density and transmits x-rays more poorly than the same thickness of the other glasses.

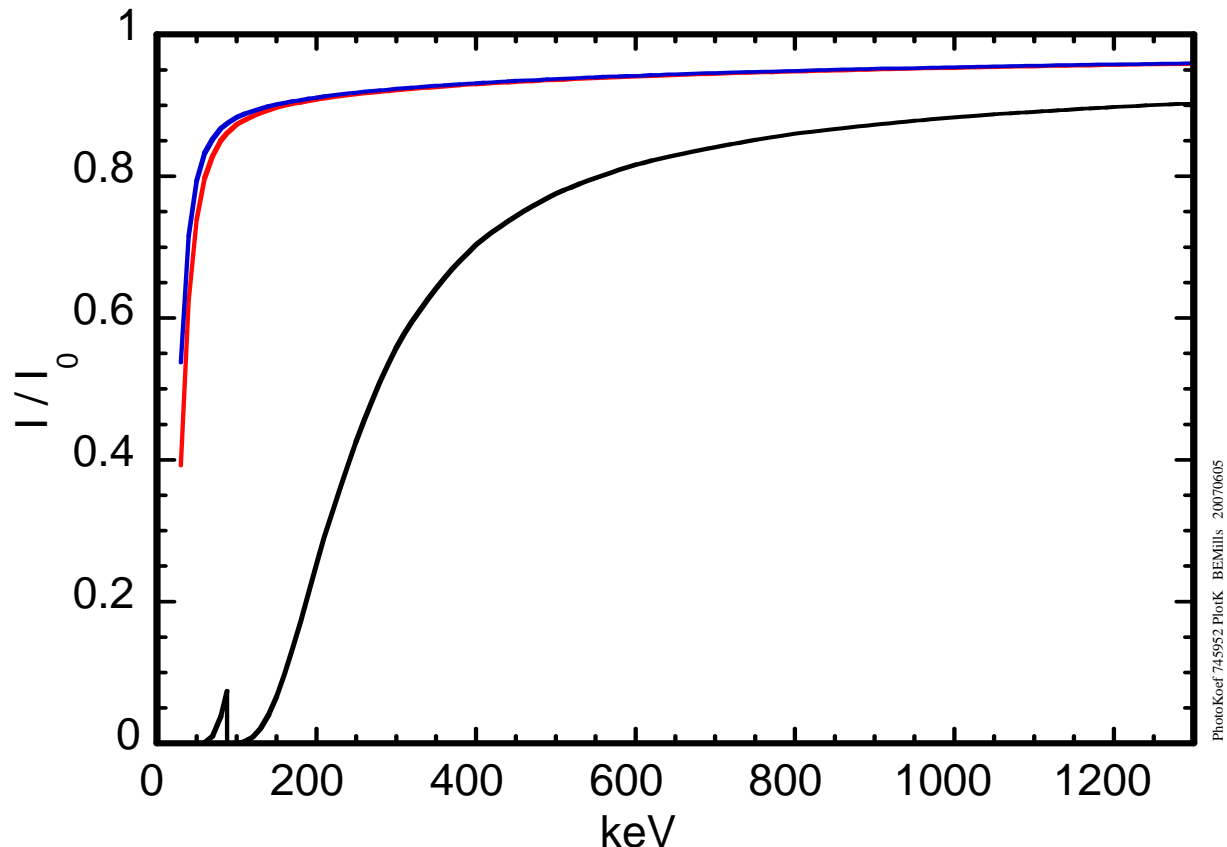


Figure 9. Transmission function for (from left to right) S2 glass (blue), E glass (red), and 50% lead glass (black).

Thermography results and discussion

Active thermography was performed on the spiral that was embedded in fiberglass. Figure 10 shows an optical image (A) of the sample compared with three thermographs. There are small reflective stickers in the corners in the shape of the letter L on the surface designated “front”. There is one in each corner except in Figure 10C, where there are only two stickers remaining. After Figure 10A was taken the nominally smooth back side of the sample was painted with flat black spray paint. One frame from the thermograph of the painted side is shown in (B). A small “swoosh” is seen just to the right of the center where some of the paint is missing. Although the embedded wires can be seen, the image is confounded by some circular artifacts that appear as prominent as the actual embedded objects. The origin of these artifacts can be seen when the paint is removed from the flat surface of the back of the sample and another image taken (C). The paint remains in the recesses caused by the texture on the surface where the fiberglass rested as it cured. Figure 10C also shows how prominent the embedded metallic objects appear when there is no paint on the surface. Interestingly, there are numerous voids in the plastic that are on the same size scale as the wire but that are not seen in the thermograph. They are more easily seen in a magnified optical image of the sample (Figure 11). Figure 10D shows an active thermography image of the unpainted front side of the sample. The “swoosh” is again visible as is the wire as a negative rather than positive signal. The wires are not as prominent as they are in the unpainted sample.

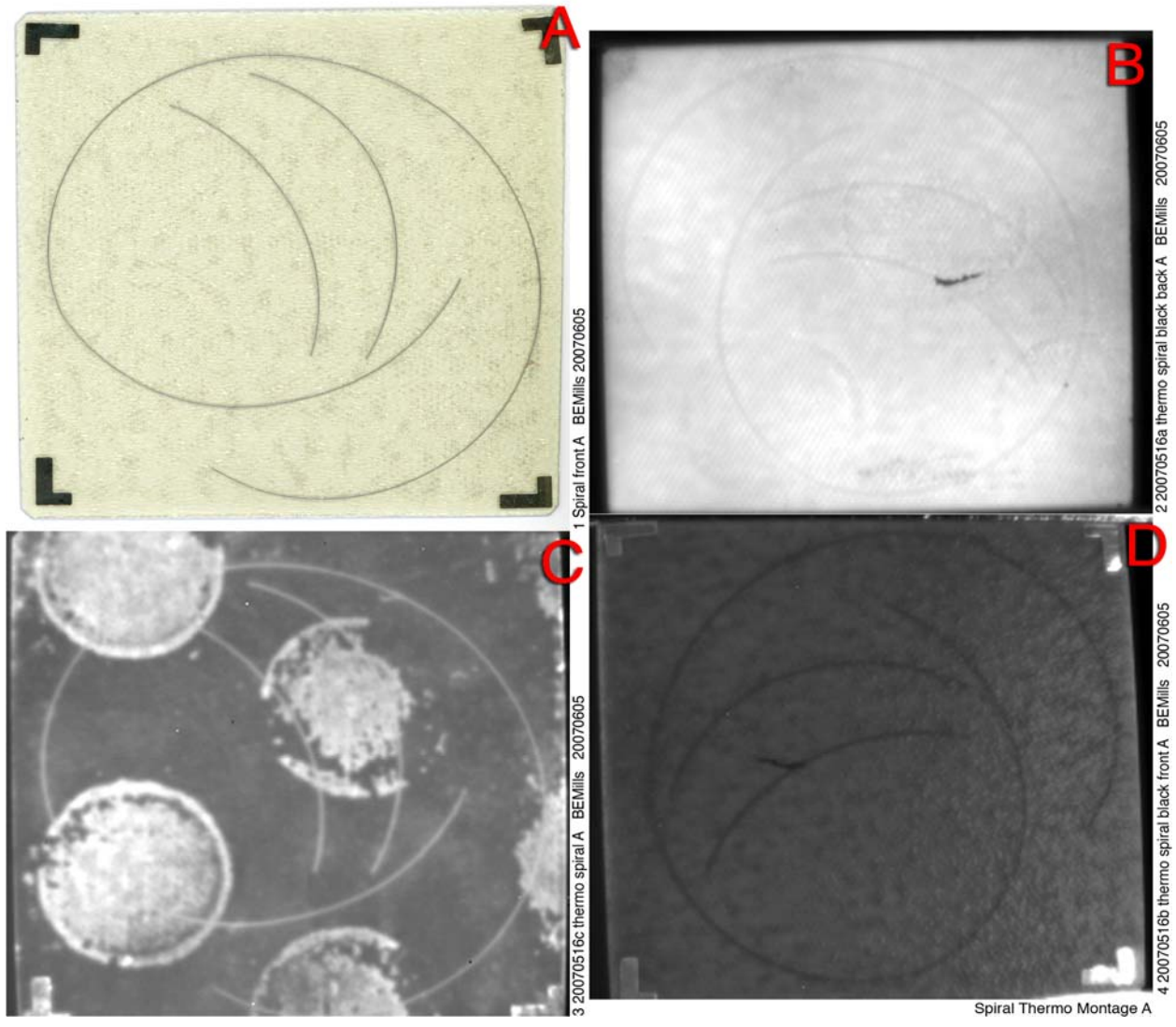


Figure 10. Optical image and active thermographs of Al 2024-O wires embedded in fiberglass. A: optical image of “front” side. B: Thermograph of “back” side after applying black paint. C: Thermograph of “front” side after most of paint has been removed. D: Thermograph of “front” side with paint on “back” side.



Spiral front bubbles A BEMills 20070605

Figure 11. Higher magnification image of object from Figure 8 showing the numerous bubbles embedded in the fiberglass that are not visible in the thermographs.

In order to understand the reason for the difference in the thermographs it is necessary to realize that, although the image is taken in the infrared, the sample is irradiated with flashlamps that emit both infrared and visible light. This light can be transmitted through, absorbed by, or reflected by the sample. The light that is absorbed can be reemitted as infrared light. The difference in relative contrast seen in the image is due to the fact that both the plastic and the voids transmit the photons, the metal reflects the photons and the paint absorbs and reradiates the photons. Where the surface that the photons first intersects is painted black several factors contribute to the image. First, the angle of irradiation and emission is not normal where the artifacts are so there is both less absorption and less emission. Where the metal is subsurface, it acts as a heat sink and reduces the emitted signal. The front side (D) also shows the effect of a different sort of texture on the signal as the angle of the surface varies from point to point. Because the embedded objects are of a known and simple shape, they can be identified. If, however, the inclusions were of unknown shape and size, these optical effects would tend to confound interpretation of the images. Obviously if the inclusions were in a transparent matrix which would yield an image like that in parts of Figure 10, there would be no need for any but optical inspection.

Conclusion

Several general conclusions can be drawn from this work:

1. Aluminum features are much more difficult to detect with x-rays than are copper features of similar size.
2. Except at the very lowest x-ray energies, the beryllium alloy tested is as easy to detect as an equivalent thickness of aluminum.
3. At the limit of detection by x-ray, even low Z contaminants such as corrosion on steel can be more apparent than small aluminum features.
4. Lead glass should be much more visible than either S2 glass or E glass.
5. Thermographic detection can be made difficult if the surface is colored and can be confounded by surface and sub-surface texture.

This page intentionally left blank.

Distribution

Internal

| | | |
|----|--------|-------------------------------|
| 1 | MS9403 | Tom Bennett, 8778 |
| 1 | MS9403 | Bob Bradshaw, 8778 |
| 1 | MS9405 | Bob Carling, 8700 |
| 1 | MS9403 | Linda Domeier, 8778 |
| 1 | MS9403 | John Hachman, 8778 |
| 1 | MS9403 | Pat Keifer, 8778 |
| 1 | MS9403 | Karen Krafcik, 8778 |
| 1 | MS9404 | Davina Kwon, 8770 |
| 1 | MS9403 | Jim McElhanon, 8778 |
| 5 | MS9403 | Bernice Mills, 8778 |
| 1- | MS9403 | Alf Morales, 8778 |
| 1 | MS9403 | April Nissen, 8778 |
| 1 | MS9403 | Timothy Shepodd, 8778 |
| 1 | MS9403 | Andrew Vance, 8778 |
| 1 | MS9403 | LeRoy Whinnery, 8778 |
| 1 | MS9403 | Bryan Wong, 8778 |
| 1 | MS9403 | Tom Zifer, 8778 |
| 2 | MS0899 | Technical Library, 4536 |
| 2 | MS9018 | Central Technical Files, 8944 |